Paper pa02-079
Submitted to the 28th International Conference on High Energy Physics
ICHEP'96, Warsaw, Poland, July 1996

Scale Dependence of the Energy Behaviour of Photon-Proton Cross Sections

H1 Collaboration

Abstract

The scale dependence of evolution of the W behaviour, the energy of the collision, of the photoproduction cross section is studied using low $Q^2 < 0.01$ GeV^2 e^+p interactions collected by the H1 experiment at HERA. The particle with the largest transverse momentum in the photon fragmentation region is used as a tag of the hard scale. The slope of the W dependence of the cross section is observed to increase steeply with the maximum transverse momentum. The result is compared both to measurements of the Q^2 evolution of the slope of the W dependence of the virtual photon-proton cross section and with Monte Carlo models. An interpretation in terms of QCD and in terms of Regge phenomenology is discussed.

1 Introduction

Measurements of the proton structure function $F_2(Q^2, x)$ in deep inelastic scattering (DIS) at HERA [1, 2] show a fast rise of F_2 with decreasing Bjorken-x, implying a fast rise of total virtual photon-proton cross section $\sigma_{tot}^{\gamma^* p}$ with the energy of the collision W. The latter can be parametrised by a simple power-law

$$\sigma_{tot}^{\gamma^* p} \propto W^{2 \cdot \lambda}, \tag{1}$$

where the parameter λ characterizes the slope of the rise of cross section. In Regge theory the slope λ can be interpreted as $\alpha(0) - 1$, where $\alpha(0)$ is the pomeron trajectory intercept, the fundamental parameter used to describe the energy evolution of elastic, diffractive dissociation and total cross sections at high energy. For real photon-proton collisions one finds a value consistent with $\lambda \approx 0.08$ [4, 5], the value found in hadron-hadron collisions [3]. For virtual photon-proton scattering however the value of λ rises from 0.2 to 0.5 when the photon virtuality Q^2 increases from 1.5 to 10^3 GeV^2. It is often argued that this change of slope is associated with a transition from a non-perturbative 'soft' to a perturbative 'hard' regime. Indeed, in the domain $Q^2 > O(5)$ GeV^2 perturbative QCD can be applied and predicts an increase of the slope λ with Q^2. In the domain of 'soft' interactions the change of slope can be explained in the Regge picture as a reduction of screening corrections with increasing Q^2 [6]. Presently pQCD and Regge theory are two complementary approaches which successfully describe physics processes in different regimes, but the transition region between these soft and hard regimes is still poorly understood. HERA provides an ideal testing ground to study the interplay between soft and hard physics, by comparing real and virtual photon-proton collisions in identical experimental conditions.

To gain more insight in this transition region we study in this paper the energy behaviour of the cross section for photoproduction events containing high p_t charged particles. The presence of a high p_t charged particle allows to identify a scale which can be varied in a similar way as in virtual photon interactions, and the effect on the energy dependence of the cross section can be studied. A continuous coverage of both the soft and hard domains becomes possible. To emulate the kinematical configuration of a $\gamma^* p$ collision as close as possible the high p_t charged track is required to be in the vicinity of the photon-quark vertex, i.e. the photon fragmentation region, which corresponds at the same time to the largest acceptance region of the H1 tracking detectors. The idea of the analysis is illustrated in Fig.1, where both the virtual and real photon processes are shown, as well as the track acceptance region.

Experimental data for this analysis were collected by H1 during the 1994 running period, in which HERA collided 27.5 GeV positrons on 820 GeV protons, thus producing e^+p interactions at $\sqrt{s} = 300$ GeV. The data sample used corresponds to an integrated luminosity of 2.6 pb^{-1}.

2 Detector and Data Sample

A detailed description of the H1 apparatus can be found elsewhere [7]. This analysis makes use of the luminosity system and the central tracking detector.

The scattered positron is detected in the electron tagger of the H1 luminosity system. The system consists of two TlCl/TlBr crystal calorimeters, installed in the HERA tunnel, each having a resolution of $\sigma(E)/E = 0.1/\sqrt{E}$ with E in GeV. The electron tagger is located at $z = -33$ m and the photon tagger at $z = -103$ m from the interaction point in the direction of outgoing positron beam. The energy scale of both calorimeters is known to better than 1.5% [8]. The acceptance of the electron tagger is confined to the kinematical range of $0.2 < y = 1 - E_{e'}/E_e < 0.8$ and $Q^2 < 0.01$ GeV^2. Here $-Q^2$ is the photon virtuality and E_e, $E_{e'}$ are the energies of the initial and scattered positrons respectively.

The charge and momentum of charged particles are measured by two coaxial cylindrical drift chambers (central jet chamber, CJC), which cover the polar angular range $15° < \theta < 165°$. Here θ is defined with respect to the proton direction. A superconducting solenoid provides a uniform magnetic field of 1.15 T parallel to the beam axis in the tracking region. The p_t and θ resolutions of the CJC are $\sigma_{p_t}/p_t \approx 0.009 \cdot p_t$ [GeV] $\oplus$ 0.015 and $\sigma_\theta = 20$ mrad [7] respectively.

Photoproduction events were triggered by a coincidence of an energy deposit larger than ~ 5 GeV in the electron tagger and one or mere track candidates with $p_t > 0.4$ GeV from the CJC trigger. In order to reduce the non-ep background contamination and to ensure a good reconstruction of the event kinematics, the following selection criteria have been applied for this analysis:

- The event vertex reconstructed from the tracks of charged particles was required to lie within ± 30 cm of the mean z-position of the interaction point, corresponding to a 3σ cut on the interaction region determined by the longitudinal size of the proton bunch.

- In order to suppress random coincidences between the high rate of Bethe-Heitler events $ep \to ep\gamma$, and p-gas background in the main H1 detector, events were rejected with a photon with $E_\gamma > 2$ GeV detected in the photon tagger, corresponding to an angular acceptance of the photon of $\theta' = \pi - \theta < 0.45$ mrad. This cut reduces also QED radiative corrections to the ep Born cross section [5].

- The y range was limited to $0.25 < y < 0.70$, to avoid regions of low electron tagger acceptance [5]. This corresponds to photon-proton collision energies $150 < W_{\gamma p} = \sqrt{ys} < 250$ GeV.

- A fiducial cut $|x_{ET}| < 6.5$ cm was applied to reject events with a positron detected close to the boundaries of the electron tagger, $x_{ET} = \pm 7.7$ cm, beyond which no good measurement of the positron energy can be provided [5].

In total $1.8 \cdot 10^6$ events satisfy the above selection criteria, from a data sample which corresponds to the integrated luminosity of $\mathcal{L} = 2.6$ pb^{-1}. The residual background contamination was estimated to be (2.4 ± 0.5)%.

The data were divided into several sub-samples (bins), according to the charged particle with the maximal transverse momentum, $p_{t,max}$, found in the pseudorapidity range $1.1 < \eta^* < 3.1$. Here the pseudorapidity is defined in the photon-proton centre of mass system as $\eta^* = -\ln(\tan(\theta^*/2))$ with θ^* measured with respect to the photon direction.

The pseudorapidity interval is limited to a region which guarantees a good track measurement in the CJC and a uniform track acceptance over the whole $W(y)$ region studied. Only those tracks were considered which have $p_t > 150$ MeV, are fitted to the primary event vertex and satisfy a number of quality criteria detailed in [9]. The systematic error due to the track selection was estimated by varying these quality criteria in a wide range and repeating the complete analysis. In total 12 bins in p_t have been defined, in a total interval ranging from 0.5 GeV to 10 GeV. The bin sizes were determined according to statistics and such that the size is always larger than four times the p_t resolution in the bin, to minimize migration effects. The values of the p_t boundaries for the bins are shown in Fig. 2.

The track reconstruction efficiency, the contamination from secondary vertices and decays close to the primary vertex, and residual bin to bin migrations have been estimated from Monte Carlo studies. Events were generated with the PYTHIA model [10] and passed through the full H1 detector simulation. All simulated events were subject to the same reconstruction and selection procedure as for real data. The migration effects were found to be small, between 10% and 20%, and the ratio of the reconstructed to the true generated events is close to one ($\pm 4\%$) in all p_t bins.

3 Results and Discussion

In ep collisions, for any subclass i of photoproduction processes the energy dependence $\sigma^i_{\gamma p}(W)$ can be extracted from the corresponding differential ep cross section, using the Weizsäcker-Williams formula [11] for the photon flux $F(y, Q^2)$. After integrating over Q^2, the corresponding relation reads:

$$\frac{dN^i_{ep}}{dy} = (1 + \delta_{RC})\ \mathcal{L}\ F(y)\ A(y)\ \epsilon^i(y)\ \sigma^i_{\gamma p}(W), \tag{2}$$

where N^i_{ep} denotes the observed number of events belonging to class i, $\mathcal{L}$ is the integrated luminosity, $A(y)$ is the acceptance of the electron tagger and $\epsilon^i(y)$ is the efficiency of the trigger and selection criteria. The factor $(1 + \delta_{RC})$ corrects the cross section for QED radiation to the ep Born cross section.

The main systematic uncertainty, which so far prevents an accurate measurement of the energy dependence of the total photoproduction cross section at HERA, is caused by to large variation of the tagging acceptance $A(y)$ (between 0.15 and 0.8 in the $W_{\gamma p}$ range of interest), which in addition strongly depends on the beam optics [5, 8]. However the *relative* energy dependence for different photoproduction event classes can be determined with much better precision. Hence we define the ratio

$$R(y) = \frac{\sigma^i_{\gamma p}(W)}{\sigma^{tot}_{\gamma p}(W)} = \frac{dN^i_{ep}/dy}{dN_{ep}/dy} \cdot \frac{\epsilon(y)}{\epsilon^i(y)} \equiv \frac{\tilde{R}(y)}{r^i_\epsilon(y)}, \tag{3}$$

where ϵ and ϵ^i denote the efficiencies for all events and for the events in bin i, and $\tilde{R}$ is the uncorrected ratio. Effectively all efficiencies in (3) were found to cancel except for the trigger efficiency. Hence r^i_ϵ is the ratio of the trigger efficiency for the sample in p_t-bin i to the one of the full sample.

The energy W dependence of the uncorrected ratio $\tilde{R}$ for each bin of p_t is shown in Fig. 2 together with a power-law fit $\tilde{R} \propto W^{2\cdot\tilde{\lambda}(p_t)}$.

In order to obtain the energy dependence of the $\sigma_{\gamma p}(W, p_t) \equiv \sigma^i_{\gamma p}(W)$ in (3) the parameters $\tilde{\lambda}(p_t)$ have been corrected for trigger trigger efficiency $r_\epsilon(y)^i$ and for the energy dependence of the total cross section in the denominator of (3):

$$\lambda(p_t) = \tilde{\lambda}(p_t) - \lambda_\epsilon(p_t) + \lambda_{I\!P} \qquad (4)$$

with $\lambda_{I\!P} = 0.08 \pm 0.03$ and $\lambda_\epsilon(p_t)$ is the trigger efficiency correction factor. The rather conservative error assigned to this value accounts for the invisible part of the total γp cross section with the data selection of this analysis (mainly elastic and low mass diffractive dissociation processes) [5]. The correction due to the trigger efficiency was obtained directly from the data, using a subsample taken with a trigger based solely on calorimetric quantities. The contributions of the systematical errors to $\delta\lambda$, additionally to the overall uncertainty in $\lambda_{I\!P}$, are summarized in the Table 1. The rightmost column gives the systematic error resulting from the stability of the power-law fit to variations of the W^2 range used.

Table 1: Systematic error summary for the measurement of the slope λ
The overall contribution $\delta\lambda_{I\!P} = 0.03$ is not included in this table, but is included in Fig.3.

Bin	$< p_t^2 >$ [GeV^2]	$\lambda \pm \delta\lambda_{stat}$	Systematical errors		
			track sel.	trigger	W^2 fit
1	0.36	0.080 ± 0.006	0.001	0.02	0.006
2	0.56	0.121 ± 0.009	0.001	0.01	0.008
3	0.80	0.157 ± 0.007	0.001	0.01	0.007
4	1.29	0.211 ± 0.008	0.002	0.01	0.004
5	2.06	0.267 ± 0.012	0.001	0.01	0.004
6	3.14	0.334 ± 0.015	0.001	0.01	0.007
7	4.90	0.344 ± 0.022	0.001	0.01	0.003
8	7.77	0.407 ± 0.031	0.001	0.01	0.006
9	12.46	0.484 ± 0.051	0.015	0.02	0.008
10	19.56	0.565 ± 0.079	0.036	0.03	0.004
11	33.43	0.603 ± 0.105	0.071	0.07	0.062
12	66.42	0.889 ± 0.192	0.135	0.08	0.122

The final corrected values of λ are plotted in Fig.3a against the scale, in view of Fig.1 chosen to be $(2p_t)^2$. The inner error bars show the statistical errors, while the full error bars correspond to statistical and systematic errors added in quadrature. The statistical errors dominate the precision of the λ measurement in high-p_t range ($p_t > 3$ GeV).

A fit to the data of $\lambda = C \cdot ln(4p_t^2) + \lambda_0$ with full errors except for $\delta\lambda_{I\!P}$ (full straight line on Fig.3a) gives a $\chi^2/ndf = 0.3$ with $C = 0.112 \pm 0.007$ and $\lambda_0 = 0.031 \pm 0.014$. Note that when the scale $4p_t^2$ is multiplied with a number, this does not change the slope C of the 'scale' dependence, but only influences the value of λ_0. Hence the change of λ with the scale is very significant.

Fig.3a shows also predictions of a longitudinal phase space model and of the PYTHIA model [10], based on perturbative QCD. As expected pure phase space effects start to become important only at very large p_t values [1] and cannot explain the trend observed in the data. PYTHIA on the other hand describes the data quite well. In studying the different ingredients in this model it turns out that the main part of the effect can be explained by the properties of the leading order QCD matrix elements. Parton showers, simulating NLO effects, as well as multiple parton-parton scattering account for at most 20% of the measured $\lambda(p_t)$ dependence. The effect due to structure functions is found to be very small hence the slope is not associated with the growth of the gluon density in the proton at small-x.

In Fig.3b the measurement of λ according to eq. (1) is shown for the virtual-photon proton cross section as function of the virtuality Q^2 as published recently in [1]. In the case of DIS the Q^2 dependence of λ is qualitatively quite well described by perturbative QCD, as shown by the values calculated for two quite different proton structure function parametrisations [12, 13]. Both parametrisations are based on the DGLAP evolution equations [14] but assume a different x-behaviour at the starting scale, Q_0 of the evolution. At $Q^2 \sim 5$ GeV^2 the D0' parton densities are flat in x ($\lambda = 0$), while for GRV they are singular ($\lambda > 0$). This difference leads to shift of the overall normalization for the GRV and D0' predictions in Fig. 3b. However, they both have a similar rise of λ with Q^2, resulting from the singular behaviour of the DGLAP evolution kernel [15].

A clear similarity between the results on high-p_t particle photoproduction and deep inelastic scattering. This can be understood as follows:

- Experimentally: an increase of Q^2 gives rise to an increase of average p_t of charged particle in the photon hemisphere as observed [17]. Hence one can enrich an event sample with high p_t particles either by selecting directly on the p_t of the charged tracks – as done in this paper for the total photoproduction event sample – or by selecting events with a high Q^2 as done in DIS. Both selections are now found to lead to event samples with a qualitatively similar evolution of the W cross section.

- Regge approach: In Reggeon Field Theory, high energy particle interactions are described by pomeron exchange and the slope λ is related to the pomeron trajectory intercept. At high energies the total interaction cross section is dominated by one-pomeron exchange and unitarity corrections, which effectively reduce the cross section value, become important. It was shown [6] that these reduce the value of λ. In both cases the selection of high p_t events and increasing Q^2 the cross sections are far below the unitarity bound [16] where unitarity corrections become gradually smaller [6]. Hence the cross section can rise faster with W for either increasing p_t or Q^2. The data shows that this is indeed the case and the development of the rise is similar.

- Parton model approach : As was shown above, the rise of the cross section of photopproduction of high p_t particles can be explaned in terms of parton–parton scattering (minijet model). On the other hand the rise of the slope due to QCD evolution in DIS is related to a singularity in the box diagram describing the elastic $\gamma^* p$ scattering amplitude. This diagram give the contribution to the $\gamma^* p$ cross section of photon parton scattering with gluon or quark radiation and has similar properties as those for parton–parton scattering in high p_t photoproduction. Hence, in view of Fig. 1, the cross section evolution with the scale is expected to be similar for both 'processes'.

[1] Mainly for that reason the last 12-th p_t bin was excluded from the final result presented in Fig.3a.

In short, a interesting similarity is observed in the evolution of the energy dependence of the $\sigma_{\gamma p}(W, p_t^2)$ and $\sigma_{\gamma^* p}(W, Q^2)$, in qualitative agreement with QCD and Regge theory expectations. The different scales used for the study of this effect in the two processes, prevents however a quantitative comparison. The range of the scale is varied from 1 GeV^2 to 100 GeV^2, showing a smooth transition from soft to hard processes.

4 Conclusion

A significant change is measured in the energy dependence of the partial cross sections $\sigma_{\gamma p}(W, p_t^2)$ with increasing transverse momentum of the charged particles in the photon fragmentation region. This result cannot be described by simple kinematical (phase space) effects. A remarkable similarity is observed in the evolution of the energy dependence of the $\sigma_{\gamma p}(W, p_t^2)$ and $\sigma_{\gamma^* p}(W, Q^2)$. This supports a common underlying picture for real and virtual photoproduction and a smooth transition between soft and hard processes.

Acknowledgement

We are grateful to the HERA machine group whose outstanding efforts made this experiment possible. We appreciate the immense effort of the engineers and technicians who constructed and maintain the H1 detector. We thank the funding agencies for financial support. We acknowledge the support of the DESY technical staff. We wish to thank the DESY directorate for the support and hospitality extended to the non-DESY members of the collaboration.

References

[1] H1 Collab., I. Abt et al., Nucl.Phys. B407 (1993) 515;
H1 Collab., T. Ahmed et al., Nucl.Phys. B439 (1995) 471;
H1 Collab., S. Aid et al., Nucl. Phys. **B470** (1996) 3,

[2] ZEUS Collab., M. Derrick et al., Phys.Lett. B316 (1993) 412;
ZEUS Collab., M. Derrick et al., Z.Phys. C65 (1995) 379;
ZEUS Collab., M. Derrick et al., Z.Phys. C69 (1996) 607.

[3] A. Donnachie and P.V. Landshoff., Phys.Lett. B296 (1992) 227.

[4] ZEUS Collab., M. Derrick et al., Z.Phys. C63 (1994) 391.

[5] H1 Collab., S. Aid et al., Z.Phys. C69 (1995) 27.

[6] A. Capella, A. Kaidalov, C. Merino and J. Tran Thanh Van, Phys.Lett. B337 (1994) 358.

[7] H1 Collab., I. Abt et al., "The H1 detector at HERA", DESY preprint 93-103 (1993), to be published in Nucl. Instr. and Meth.

[8] H1 Collab., T. Ahmed et al., Z.Phys. C66 (1995) 525.

[9] H1 Collab., S. Aid et al., DESY preprint 096-122.

[10] T. Sjöstrand, CERN-TH-6488 (1992), Comp. Phys. Commun. 82 (1994) 74.

[11] C.F. Weizsäcker, Z.Phys. 88 (1934) 612;
E.J. Williams, Phys.Rev. 45 (1934) 729;
S. Frixione et al., Phys.Lett. B319 (1993) 339.

[12] M. Glück, E. Reya and A. Vogt, Z.Phys. C67 (1995) 433;
A. Vogt, Proceedings of the Workshop on Deep-Inelastic Scattering and QCD, Paris (1995) 261.

[13] A.D. Martin, R.G. Roberts and W.J. Stirling, Phys.Lett. B306 (1993) 145.

[14] V.N. Gribov and L.N. Lipatov, Sov.J.Nucl.Phys. 15 (1972) 438;
G. Altarelli and G. Parisi, Nucl.Phys. B126 (1977) 298.

[15] John C. Collins (Illinois Tech. and Argonne), Print-86-0298 (ILLINOIS TECH), Jan 1986. 12pp. Presented at SSC Workshop, Los Angeles, CA, Jan 15-24, 1986. Published in UCLA SSC Workshop 1986:15 (QCD184:U2:1986)

[16] E. Levin, hep-ph/9607210 (1996).

[17] H1 Collaboration, I Abt et al., Z.Phys.C63 (1994) 377

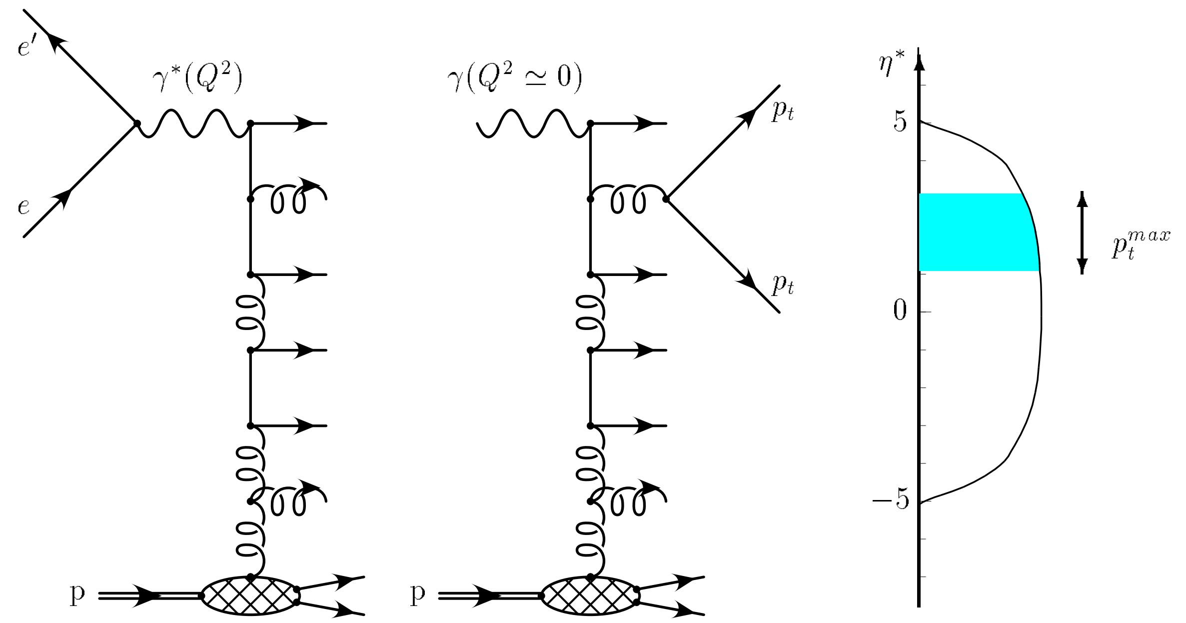

Figure 1: Feynmann diagrams for D.I.S. event and photoproduction event with high p_t particles (jets) in the final state. The sketch on the righthand side illustrates an inclusive charged particle pseudorapidity distribution in γp centre of mass system, with the range used to search for high p_t tracks.

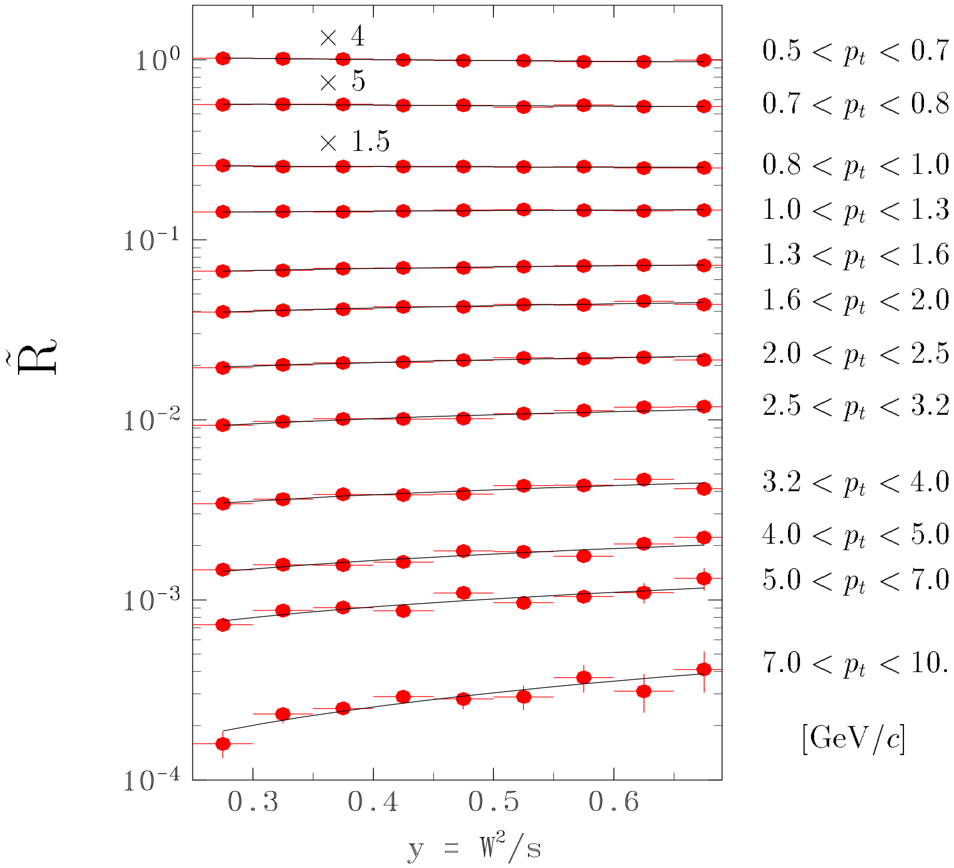

Figure 2: The energy dependence of the ratio $\tilde{R}$ in different bins of the maximum p_t of the charged particles produced in the pseudorapidity window $1.1 < \eta^* < 3.1$. The curves represent a Regge motivated fit of the form $\tilde{R} \propto W^{2 \cdot \tilde{\lambda}}$.

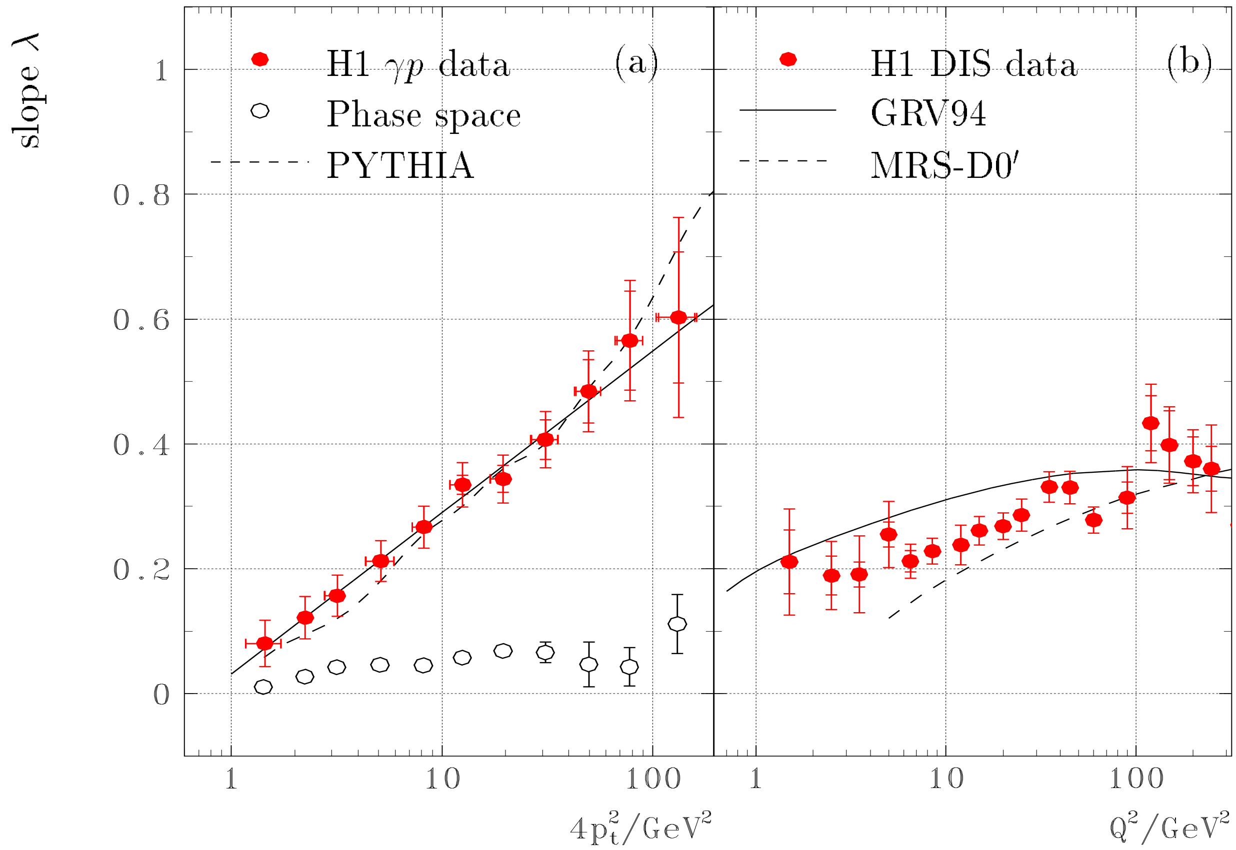

Figure 3: a) The 'scale' dependence of the slope λ in a) photoproduction. The full line represents the result of the linear fit $\lambda = C \cdot ln(4p_t^2) + \lambda_0$ to the data. b) The 'scale' dependence of the slope λ in deep inelastic data compared to different parametrisations of the proton structure function F_2.